Front. Struct. Civ. Eng. 2024, 18(4): 536–550
https://doi.org/10.1007/s11709-024-1013-2

RESEARCH ARTICLE

Crack identification in concrete, using digital image correlation and neural network

Jingyi WANG, Dong LEI*, Kaiyang ZHOU, Jintao HE, Feipeng ZHU, Pengxiang BAI

College of Mechanics and Materials, Hohai University, Nanjing 211100, China
**Corresponding author. E-mail: leidong@hhu.edu.cn*

ABSTRACT In engineering applications, concrete crack monitoring is very important. Traditional methods are of low efficiency, low accuracy, have poor timeliness, and are applicable in only a limited number of scenarios. Therefore, more comprehensive detection of concrete damage under different scenarios is of high value for practical engineering applications. Digital image correlation (DIC) technology can provide a large amount of experimental data, and neural network (NN) can process very rich data. Therefore, NN, including convolutional neural networks (CNN) and back propagation neural networks (BP), can be combined with DIC technology to analyze experimental data of three-point bending of plain concrete and four-point bending of reinforced concrete. In addition, strain parameters can be used for training, and displacement parameters can be added for comprehensive consideration. The data obtained by DIC technology are grouped for training, and the recognition results of NN show that the combination of strain and displacement parameters, i.e., the response of specimen surface and whole body, can make results more objective and comprehensive. The identification results obtained by CNN and BP show that these technologies can accurately identify cracks. The identification results for reinforced concrete specimens are less affected by noise than those of plain concrete specimens. CNN is more convenient because it can identify some features directly from images, recognizing the cracks formed by macro development. BP can issue early warning of the microscopic cracks, but it requires a large amount of data and computation. It can be seen that CNN is more intuitive and efficient in image processing, and is suitable when low accuracy is adequate, while BP is suitable for occasions with greater accuracy requirements. The two tools have advantages in different situations, and together they can play an important role in engineering monitoring.

KEYWORDS digital image correlation, convolutional neural network, back propagation neural neural network, damage detection, concrete

1 Introduction

Concrete is widely used in bridges [1], tunnels [2], civil construction [3], harbor [4], and other projects, in all of which cracking is a troubling problem [5]. Multiple factors can cause cracks [6], and cracks indicate the initiation of the damage process in concrete [7]. When the tensile stress [8] is greater than the tensile strength of concrete, cracks are generated, which can be roughly divided into two types: structural cracks caused by external loads, and non-structural cracks caused by the stress originating within concrete itself [9]. Cracks weaken the strength, stability, durability of the building, and enhance permeability, thus the structure is easy to invade [10], causing steel corrosion and cement matrix weakening [11]. In recent years, various cracks detection methods have emerged. Invisible for surface crack, for example, has been applied to road tests, soil inversion of Rayleigh wave testing technique [12]. Laser-ultrasonic technology can monitor crack depth [13], unmanned aerial vehicles (UAVs) and digital image methods can be used to inspect high-level structures [14], UAVs and underwater robots can detect the high dam concrete cracks [15]. These techniques can be applied to a wider area of pulsed eddy current thermal imaging [16], at the same time as use of large-scale training data, GPU, the development of artificial intelligence, etc. Deep learning concepts introduced in the field of image recognition

Article history: Received Feb 6, 2023; Accepted Apr 11, 2023

[17], can provide image reconstruction, classification, and identification of fracture technology [18], for example, according to the road image grayscale image classification pavement [19], the data set partitioned with cracks shape, etc. [20]. These technologies can help to more accurately identify visible cracks on the surface of a structure.

In addition, various algorithms have sprung up to train neural network (NN), which aim to produce models with accurate predictions. Among these, decision tree algorithms (GBDT) [21], VARANS-VOF [22], modeling interactions of wave and perforated breakwater by means of gradient boosting. Through combining numerical data with experimental data [23], it is possible to calculate the optimal empirical coefficient related to linear and nonlinear drag force coefficients. With limited samples, the GBDT model can still identify the trend in nonlinear influence of model parameters [24]. Based on a unified framework of higher-order shear deformation theory [25] and modified couple stress theory, combined with artificial neural network (ANN) and balancing composite motion optimization (BCMO) [26], it is possible to solve the optimization problem relating to vibration and buckling of functionally graded porous microplates [27] with uncertain material properties. The random vibration and buckling behavior can be predicted [28].

Regarding damage detection, the combination of NN and other methods can identify structural damage more accurately. Based on the two-dimensional (2D) curvature mode shape method, convolutional neural networks (CNN) and Faster Region-based CNN [29] (region-based faster R-CNN), the damage to plate structure can be detected. CNN is trained to be able to predict the type of damage, and the faster R-CNN can predict the boundary box around the area of damage [30]. In the stochastic-based coupled model for damage identification model of plate structures, the damage identification index based on the derivative of mode shape is applied to the damage location of unfixed plate structures. Using antlion optimizer (ALO) [31] instead of the back propagation (BP) algorithm, data on the mean square error (*MSE*) [32] is used to find the best initial value of the learnable parameters of the ANN, and these parameters are added to the NN for damage recognition. The results show that the damage index combined with ALOANN has better performance compared to using ANN alone, even when noise level is added to the modal characteristics [33]. For heterogeneous porous media, a stochastic deep collocation method (DCM) is presented based on neural architecture search and transfer learning. The hyper-parameters of the network are determined and optimized, and transfer learning techniques are used to reduce the computational cost [34]. For three-dimensional potential problems in non-homogeneous media, a DCM is proposed. A physics-informed NN with material transfer learning is utilized to reduce the solution of the non-homogeneous partial differential equations to an optimization problem. Different configurations are tested and a transfer learning technique is applied to different materials, so as to improve the generality and robustness of the method [35].

CNNs [36] are widely used for image recognition. Their operation can be divided into input layer (for input image), hidden layer (including convolutional layer, pooling layer, and full connection layer), output layer, or classification layer (which can be regarded as a kind of activation function layer to classify information) [37]. A schematic CNN diagram is shown in Fig. 1.

A BP algorithm neural network is a kind of multi-layer forward NN [38], which is widely used in pattern recognition and classification, function approximation, data compression, and other fields. The BP neuron model is shown in Fig. 2.

In this paper, two-dimensional digital image processing technology and NNs are combined to identify cracks on concrete surfaces. Based on a three-point bending

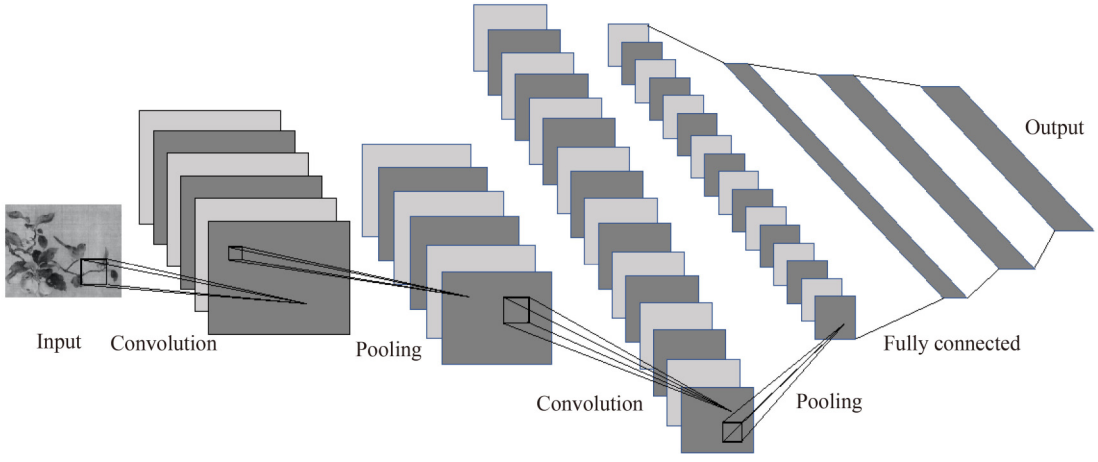

Fig. 1 Schematic diagram of the CNN.

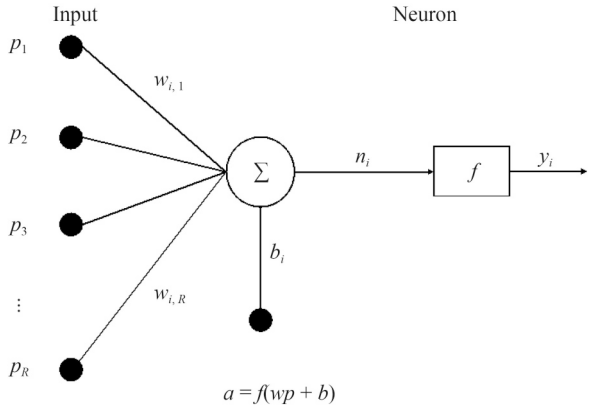

Fig. 2 Example of a BP neuron model.

experiment of plain concrete and a four-point bending experiment of reinforced concrete, a strain nephogram and a pure digital matrix containing various parameters are obtained by digital image correlation (DIC) technology, and the latter are saved as mat files. The CNN and the BP are trained respectively to obtain a judgment index graph for crack identification; these graphs are compared with the actual situation and with each other. The research structure of this paper is shown in Fig. 3.

Since DIC technology can obtain a large amount of experimental data, and NNs can handle very rich data, use of NN is combined with DIC technology to analyze the rules in the large amount of data. In addition to using strain data for training, displacement data are added for comprehensive consideration, which makes the crack monitoring results more objective and comprehensive. Moreover, CNN and BP are used for comprehensive research to compare the training and recognition effect of cloud map and pure digital matrix methods. The two methods complement and verify each other. They can embody their advantage in different situations, and have application value for practical engineering.

2 Methodology

To achieve a more objective and comprehensive study, it is necessary to record a large amount of data in relevant experiments through DIC technology to provide to different NNs for training, so as to find rules in the data. In addition, it is necessary to make comprehensive analysis, combine strain and displacement parameters, and compare the identification results of the NNs. This chapter reports on relevant experiments carried out to obtain the required samples, which are divided into two parts. The first part of the chapter narrates the production of samples in three-point bending and four-point bending experiments, including size, proportion and speckle, and then illustrates the instruments used in the experiment. The second part illustrates the loading process and the condition of specimens in the three-point bending and four-point bending experiments.

2.1 Experiment

2.1.1 Production of specimens for testing

Cuboid specimens are used in this experiment. After pouring, the specimens are cured for 28 d under standard conditions, and then the bending test is carried out. In the three-point bending test, plain concrete specimens with an initial size of 100 mm × 100 mm × 300 mm are used. In the four-point bending test, reinforced concrete specimens are used, as shown in Fig. 4.

Natural granite stone is used for aggregate in concrete specimens, medium sand is used, and PO42.5 ordinary Portland cement is used for mortar. The ratio of concrete is shown in Tables 1 and 2.

For the three-point bending test, the natural speckles on the surface of the concrete specimen are not ideal. Due to the small size of the specimens, white paint is first

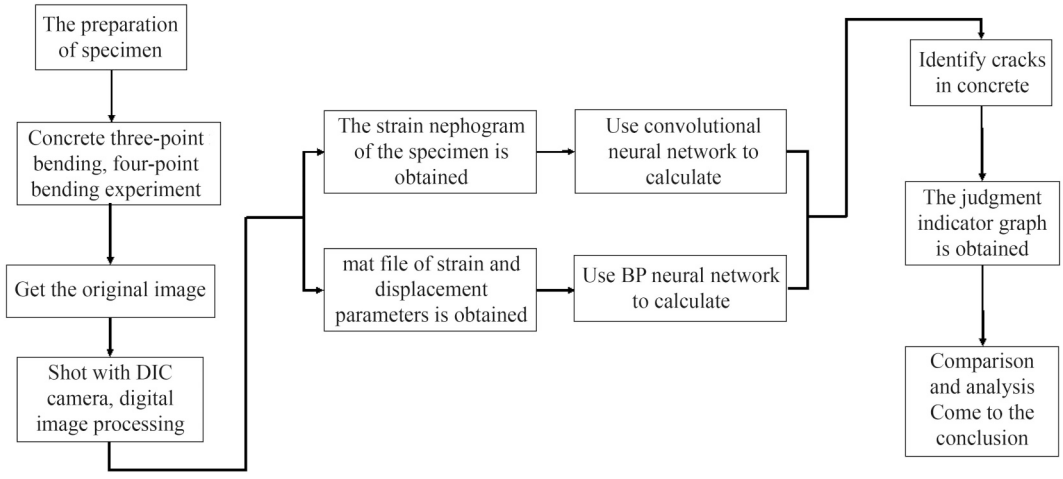

Fig. 3 Schematic diagram of research ideas.

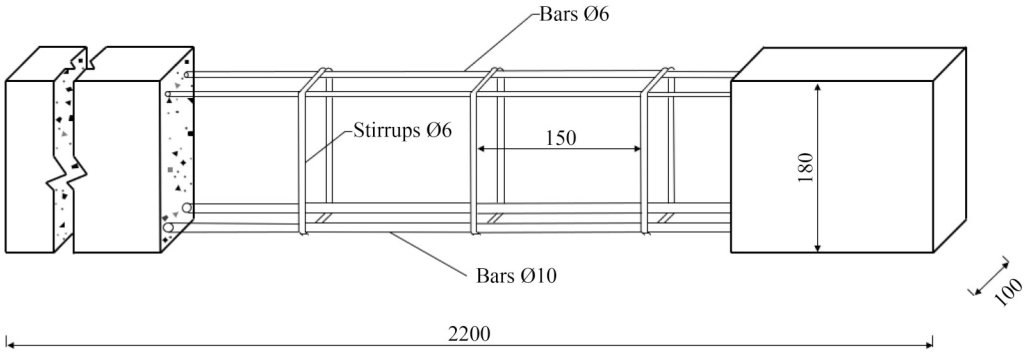

Fig. 4 Four-point bending concrete specimen.

Table 1 Three-point bending test concrete ratio

Mix proportion	Material utilization amount (kg/m^3)		
	Cement	Water	Aggregate
1:0.5:5	369	185	1846

Table 2 Four-point bending test concrete ratio

Concrete strength（MPa）	Concrete mix proportion			
	Cement	Sand	Rubble	Water
25.2	355	640	1235	185

sprayed on the surface of the specimen to provide a uniform background color, after the white paint has dried black paint is scattered randomly on the white surface to form speckles. The results of the process are shown in Fig. 5.

For the four-point bending test, although paint spraying provides even speckle distribution, the spray paint speckle size is too small compared to the specimen size. So speckles are randomly drawn on the surface of the specimen with a marker.

2.1.2 Experimental devices

The compression and bending experiment uses CSS44100 100 kN electronic universal testing machine produced in Changchun Testing Machine Research Institute. The image acquisition system is mainly an MV-VD120SC industrial CCD camera with a resolution of 1280 × 960 pixels, and equipped with a Japanese Computer million-pixel lens, model M0814-MP. An LED light source is used in the experiment. The complete experimental system is shown in Fig. 6.

2.2 Loading process

2.2.1 Three-point bending test of concrete specimens

Plain concrete specimens are used in the three-point bending test. The load curve and the displacement curve are shown in Fig. 7, where the black solid line is the load curve, and the red dotted line is the displacement curve.

Fig. 5 Speckle fabrication of three-point bending test specimen.

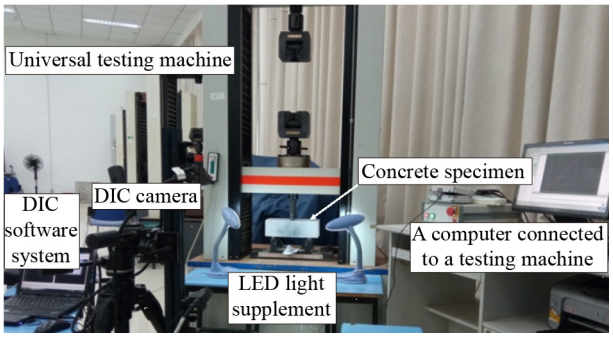

Fig. 6 Experimental system installation.

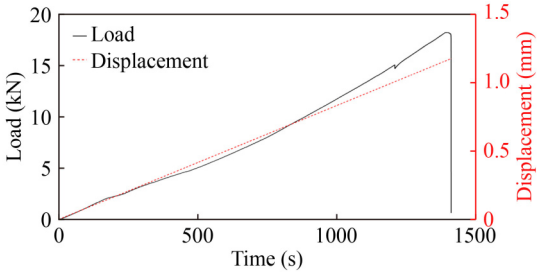

Fig. 7 The load curve and the displacement curve.

The strain nephogram of the first principal strain is obtained by processing the speckle image of the specimen surface taken by DIC camera. Brighter areas mean more damage. Therefore, the distribution of the damage on the surface of experimental specimens can be intuitively seen through the different colors of the strain nephogram. The brighter the color, the greater the damage.

After observing the strain nephogram, during the 1315.5 s of the experiment, visible cracks appear in the

strain nephogram of the concrete specimen, as shown in Fig. 8(a), and the color bar is shown on the right. At this time, the corresponding load is 16.877 kN and the displacement is 1.095 mm.

At 1406.5 s, the specimen becomes completely destroyed. At this time, the corresponding load is 18.114 kN and the displacement is 1.171 mm, as shown in Fig. 8(b), and the color bar is shown on the right.

It can be seen that with the increase of load, there is only one main crack, which starts from the upper right corner of the specimen and expands to the left until the specimen is completely destroyed.

2.2.2 Four-point bending test of concrete specimens

In the four-point bending test, the reinforced concrete specimens are uniformly loaded from 0 to 13 kN.

When the load is 3 kN, cracks in the strain nephogram become obvious and dark cracks appear in the strain nephogram, as shown in Fig. 9.

When the load is 13 kN, the microscopic cracks in the strain nephogram expand and bright cracks appear in the strain nephogram, as shown in Fig. 10.

When the load continues to increase, the specimen becomes completely destroyed, as shown in Fig. 11.

It can be seen that with the uniform increase of load, cracks appear on both sides of the specimen first, and then crack in the middle. Cracks start at the bottom and extend upward until the specimen is completely destroyed.

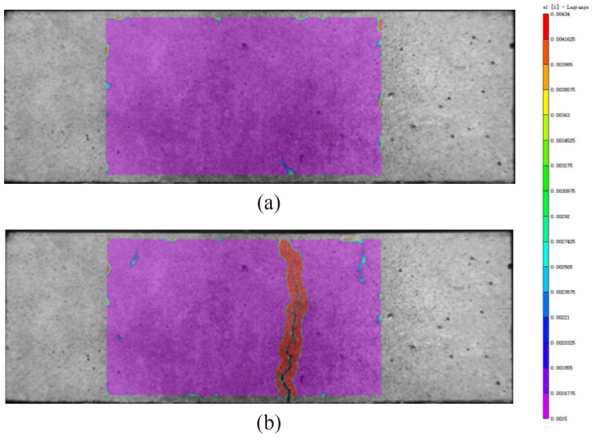

Fig. 8 The first principal strain nephogram: (a) cracks appear in the strain nephogram; (b) the specimen becomes completely destroyed.

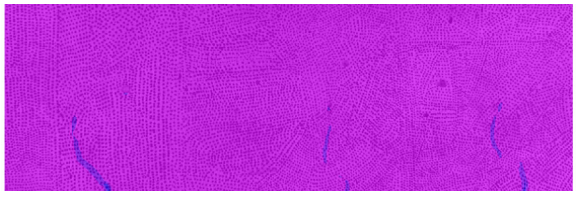

Fig. 9 The strain nephogram corresponding to the load of 3 kN.

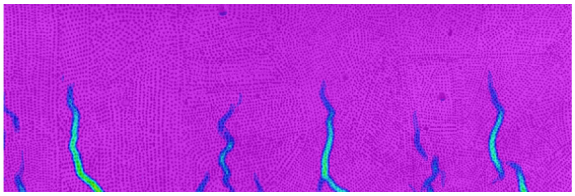

Fig. 10 The strain nephogram corresponding to the load of 13 kN.

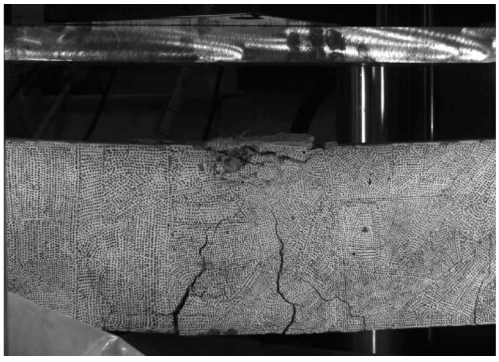

Fig. 11 Specimen complete failure.

3 Result and discussion

With a lot of data from the DIC technology, the application of a neural network for analysis can be more objective, and the combination of strain and displacement parameters can make judgments more comprehensive. To make damage recognition applicable to more scenarios, the results of a different network training process are compared and analyzed. This chapter combines the data obtained from DIC analysis with the output of the neural network to introduce a method of judging whether a concrete specimen cracks. CNN and BP are trained to judge and recognize the three-point bending test and the four-point bending test respectively, and the judgment index graphs are obtained. In addition, the composition of CNN used, the selection and grouping of the experimental data, that is, the division of training set and verification set, as well as the analysis results of CNN and BP are introduced, and the two methods are compared. They each have advantages and disadvantages, and have different applications in different situations. The results offer some opportunities for engineering application.

3.1 Three-point bending test of concrete specimen

3.1.1 Using convolutional neural networks to identify cracks in concrete three-point bending

First of all, it is necessary to introduce the CNN

architecture. GoogLeNet is a pre-trained 22-layer CNN, and the Inception structure is studied from the "Network in Network" model. Compared with the popular AlexNet [39] and VGGNet [40], GoogLeNet [41] can obtain better training effect due to fewer layers of NN structure, which enables GoogLeNet to make more efficient use of computer hardware resources. More features are extracted with the same amount of computation [42]. Therefore, the pre-trained GoogLeNet is used in this paper to extract crack features from strain nephograms of concrete specimens. In addition, there are more robust EfficientNet [43] models that increase the width, depth and resolution, thus higher fine-grained features can be recorded and the system is easier to train. However, for shallow networks with large width, it is often difficult to learn deeper features, and the network becomes deeper.

Details of GoogLeNet used in this paper is shown in Table 3. It is possible to use multi-class classifications, for example, the cracking grade of concrete, spalling problem and corrosion problem [44–46], so the softmax function is utilized.

Data selection and division are introduced in the following paragraph. During the experiment, the DIC camera takes pictures every 0.5 s. A group of typical

Table 3 The detailed information of GoogleNet

Type	Name	Size	Step size and remarks	Quantity
Input	ImageInput	224 × 224 × 3		1
Convolution layer	Convolution2d	7 × 7 × 3	[2 2]	1
		1 × 1 × 64	[1 1]	1
		3 × 3 × 64	[1 1]	1
		1 × 1 × 192	[1 1]	4
		5 × 5 × 16	[1 1]	1
		3 × 3 × 96	[1 1]	2
		1 × 1 × 256	[1 1]	4
		3 × 3 × 128	[1 1]	2
		5 × 5 × 32	[1 1]	1
		1 × 1 × 480	[1 1]	4
		5 × 5 × 16	[1 1]	1
		1 × 1 × 512	[1 1]	12
		5 × 5 × 24	[1 1]	2
		3 × 3 × 112	[1 1]	1
		5 × 5 × 32	[1 1]	3
		3 × 3 × 144	[1 1]	1
		1 × 1 × 528	[1 1]	4
		3 × 3 × 160	[1 1]	2
		1 × 1 × 832	[1 1]	8
		5 × 5 × 48	[1 1]	1
		3 × 3 × 192	[1 1]	1
Pooling layer	MaxPooling2	3 × 3	[2 2]	4
		3 × 3	[1 1]	9
	GlobalAveragePooling2			1
Normalization	CrossChannelNormalization		Each element has five channels	2
	Dropout		40% discarded	1
Activiation layer	Relu			57
The depth of the series	DepthConcatenation		Four input	9
Fully connected layer	FullyConnected			1
Output layer	Softmax			1
	Classification		Classification of output	1

experimental data are selected, starting with the first photo taken by DIC camera, 0.5 s after the experiment begins. As the changes of specimens are very small at the beginning, one research data picture is selected every five seconds, namely the first, 11th, and 21st... pictures taken by DIC camera, with the load uniformly loading. By the time of the 2711th DIC photo, the crack propagation of the specimen is faster. One DIC camera picture is selected every 0.5 s, namely the 2711th, 2712th, 2713th, ..., as the 272nd, 273rd, and 274th pictures in the research data, until the specimen is completely cracked. A total of 381 research data images are obtained, corresponding to the loading process of 0–18 kN.

The images in the data are arranged according to the time sequence in the experiment process, and a total of 381 strain nephograms are obtained after processing. After checking, the last three strain nephograms, where specimens are completely destroyed, are removed; a total of 378 strain nephograms are available. The first 50 intact strain nephograms without cracks are labeled as "negative," corresponding to the number 0, with the load of 0–2.628 kN. The last 50 strain nephograms with the most evident cracks are labeled as "positive," corresponding to the number 1, with the load of 18.1 kN. These 100 strain nephograms are selected as the training set to train the designed CNN, and the middle segment of the data, 278 in total, is selected as the verification set. The trained CNN is used to identify the verification set to judge the cracking of three-point bending test specimens. The data partitioning is listed in Table 4.

In the training, the network is trained to obtain a value between [0,1] on the DIC image of a specimen as the judgment indicator, and the distance between the value of this indicator, 0 and 1, respectively represented the degree of approaching "negative" and "positive." The smaller the indicator is, the lower the damage degree is and the closer the specimen is to intact. On the contrary, the larger the indicator is, the more obvious the crack development is on the specimen surface.

The following is about the results and the analysis. After using the trained CNN to recognize the validation set, the results are shown in Fig. 12.

MSE is 2.615952379 and the Root Mean Squared Error (*RMSE*) is 1.617390608.

The abscissa is the load size and the sample number, which in turn correspond to the data in the verification set, that is, in the 51–338 datasheets. Sheet 51 corresponds to sample number 1, and so on. It can be found that the indicator obtained at the beginning is very stable. Starting from specimen numbered 210, with a load of 16.537 kN, the judgment indicators begin to fluctuate. The indicator begins to remain above 0.7 at specimen number 227. In addition, the cracks visible to human eyes occurred at sample No. 214, while the judgment indicator of the CNN fluctuated at sample No. 210. It can be seen that the well-trained CNN can effectively predict cracks and give early warning of failure. After the image is rotated, the CNN is used for training and recognition under the same conditions again. After comparison, the image of the judgment indicator obtained remains unchanged.

Table 4 Data partitioning of CNN

Content information	Training set (100 in total)	Verification set (278 in total)
Number of strain nephogram	1–50, 329–378	51–328
Load process (kN)	0–2.628, 18.1	2.686–18.072
Judgment indicator	0 (negative), 1 (positive)	To identify [0,1]

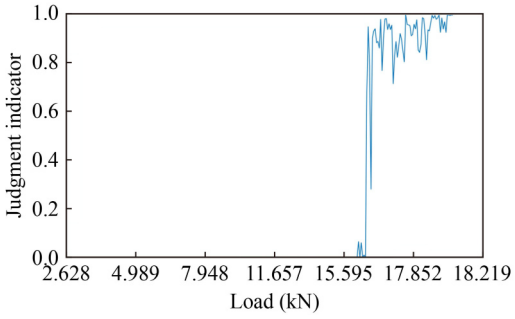

Fig. 12 The judgment curve of CNN.

Meanwhile, sample No. 210 corresponds to strain nephogram No. 260, with a load of 16.537 kN, as shown in Fig. 13(a).

It can be seen from the strain nephogram that the crack is not evident at the time of sample/specimen No. 210, only showing a little cracking trend at the upper right edge. However, the judgment indicator of the CNN is different from the steady 0 at the beginning, and fluctuates, thereby providing a warning.

Sample No. 214 corresponds to strain nephogram No. 264, with a load of 16.877 kN, as shown in Fig. 13(b). At this point, the cracks in the strain nephogram are more evident, and the judgment indicator obtained by the CNN is about to undergo a large jump.

Sample No. 217 corresponds to strain nephogram No. 267, with a load of 17.162 kN, as shown in Fig. 13(c). At this point, the judgment indicator obtained by the CNN jumps to 0.9498.

Sample No. 219 corresponds to strain nephogram No. 269, with a load of 17.281 kN, as shown in Fig. 13(d). The judgment indicator falls to 0.2814 in this sample.

After this big fluctuation, the corresponding judgment indicator of the subsequent numbered samples begins to stabilize above 0.7, indicating evident cracks. For example, in the 277 strain nephograms, the judgment indicator is 0.7693 and the load is 17.603 kN, as shown in Fig. 13(e).

As the crack expands, it becomes more evident in the strain nephogram. For example, in the 373rd strain nephogram, the load is 18.118 kN, as shown in Fig. 13(f).

It is found that the well-trained CNN can give timely

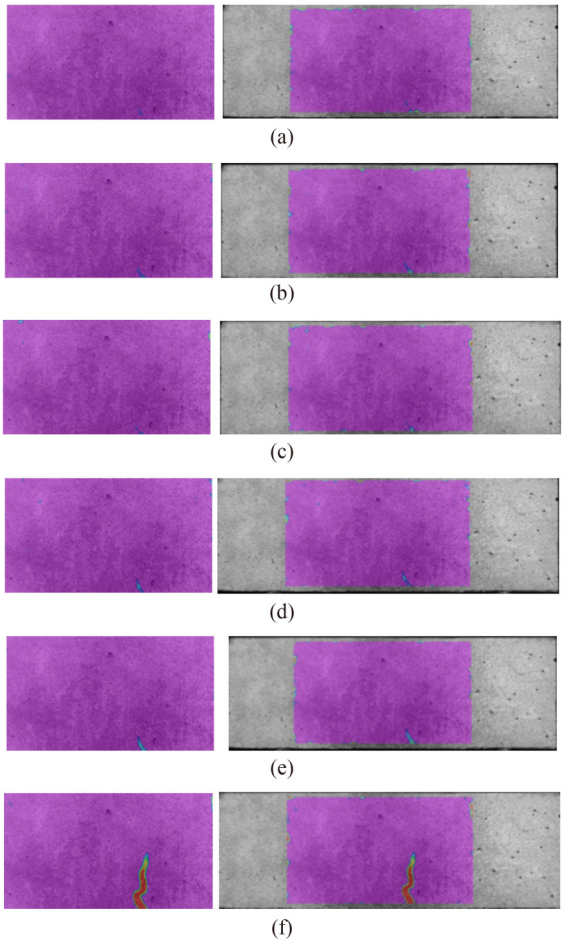

Fig. 13 The first principal strain nephograms: the strain nephogram corresponding to the load of (a) 16.537 kN; (b) 16.877 kN; (c) 17.162 kN; (d) 17. 281 kN; (e) 17. 603 kN; (f) 18.118 kN.

warning of the existence of cracks, according to the judgment indicator graph obtained from the CNN and the actual strain nephogram. The CNN can recognize that cracks in the strain nephogram as they begin to appear, and accordingly, the judgment indicator graph will fluctuate and jump. With the development of cracks, the judgment indicator image shows an upward trend, and eventually stabilizes near the maximum value. The size of the judgment indicator reflects the integrity of the specimen surface to a certain extent, and the fluctuation of the judgment indicator shows that some degree of change has taken place on the specimen surface, which provides a warning sign of cracks. In addition, the trend of the judgment indicator image is consistent with the actual crack development.

3.1.2 Using back propagation neural neural network to identify cracks in concrete three-point bending

The first principal strain ε_1, the second principal strain ε_2, the strain in x-direction ε_{xx}, the strain in y-direction ε_{yy}, the shear strain ε_{xy}, the horizontal displacement u, and the longitudinal displacement v at each point are calculated by using the specks of the concrete three-point bending specimens, imaged by DIC in different stages. DIC software is used to output the obtained data as mat files for subsequent processing with Matlab. The file is a matrix composed of each pixel, the numbers of rows and columns of the matrix corresponds to the coordinates of a pixel, and each number in the matrix is the corresponding information, namely displacement or strain.

The BP neural network is constructed to identify concrete damage. At the beginning of training, the weight is random. The momentum factor is 0.03, the learning rate is 0.01, the error tolerance is 0.01, and the maximum iteration is 2000. The hyper-parameters of the BP are listed in Table 5. When the momentum factor and learning rate are too large, the BP neural network will easily fall into the local minimum, which will make the BP unable to fit the data well. When the momentum factor and learning rate are too small, the learning speed of the BP neural network is slow and cannot converge quickly, so the selection of momentum factor and learning rate needs to be adjusted appropriately. Iteration is stopped when the sum of error squares is less than error tolerance, otherwise, the maximum iterations is reached, and then iteration is stopped.

Table 5 The hyper-parameters of the BP

Hyper-parameters	Value
Momentum factor	0.03
Learning rate	0.01
Error tolerance	0.01
Maximum iteration	20000

The selection of hyper-parameters determines the efficiency and results of training. In a gradient descent algorithm, the learning rate determines the efficiency and accuracy of the estimated parameters in the optimization process. Hyper-parameter tuning is the process of determining the correct combination of hyper-parameters that maximizes model performance. It is significant to the architecture of neural networks which will be important to prevent the model from getting stuck at local optimal.

The BP neural network is trained with different parameters, including horizontal displacement u only, longitudinal displacement v only, all displacements u, v, strain in y-direction ε_{yy}, longitudinal displacement v, strain in x-direction ε_{xx}, horizontal displacement u, and all parameters ε_1, ε_2, ε_{xx}, ε_{yy}, ε_{xy}, u, v. The selected parameters are listed in Table 6.

Excluding the data with large fluctuations, 133 mat files 1–100 and 341–373 are selected as training sets. Among them, 1–100 do not represent a cracked stage of the concrete, and are labeled as “0”; files 341–373

Table 6 Parameter selection

Number of the selected group	The first principal strain ε_1	The second principal strain ε_2	Strain in x-direction ε_{xx}	Strain in y-direction ε_{yy}	Shear strain ε_{xy}	Horizontal displacement $\boldsymbol{u}$	Longitudinal displacement $\boldsymbol{v}$
A						√	
B							√
C						√	√
D				√			√
E			√			√	
F	√	√	√	√	√	√	√

represent cracked concrete and are labeled as "1". At the same time, mat files 101–324 are selected as the verification set, 224 in total. As listed in Table 7.

The BP neural network is trained with the data of the training set, and the trained BP neural network recognizes the data of the verification set, and the recognition results are drawn to obtain the image of the judgment indicator.

The identification situation is shown in Fig. 14, where the horizontal axis is the sample label. The vertical axis is the failure degree judgment indicator, and the failure degree increases with the increase from 0 to 1. Parameters of different combinations are selected as the input of the network, and the judgment result is obtained after the operation. The closer the judgment value is to 0, the more the corresponding sample tends to select the label "0"; that is, the better it is. Conversely, the closer it is to 1, the more the corresponding sample tends to select the label "1"; that is, the crack tends to appear.

The K-fold cross validation technique is adopted to help to evaluate the model to avoid a high variance and bias in the results generated, and it helps to provide a fairer model evaluation. The MSE is 0.261614% and the RMSE is 0.511482%.

Analyzing these results can show that, selecting horizontal displacement u, and selecting strain in x-direction ε_{xx}, for these two judgment indicator images, most of the indicators of trends in line with the actual. However, there are some indicators among those with larger fluctuation, for which horizontal direction is larger than the vertical. This could be due to instability of the machine itself.

Comparing the identification results of different parameter groups in this experiment, we can see that the combination of strain and displacement parameters is better. It can be seen that this curve has higher slope, more certain recognition results, less noise impact, and less fluctuation. A higher slope of judgment curve means a more certain judgment, which is consistent with actual known behavior of brittle fracture of plain concrete.

Comparing the recognition results of the CNN and the BP, we can note that in the judgment indicator graph, the fluctuation of the CNN is sample No. 210 (the 260th strain nephogram), and the load is 16.537 kN, which corresponds to sample No. 144 in BP neural network. It

Table 7 Data partitioning of the BP

Content information	Training Set (133 in total)	Verification set (224 in total)
Number of mat files	1–100, 341–373	101–324
Load process (kN)	0–4.989, 18.1	5.058–18.051
Judgment indicator	0 (negative), 1 (positive)	to identify [0,1]

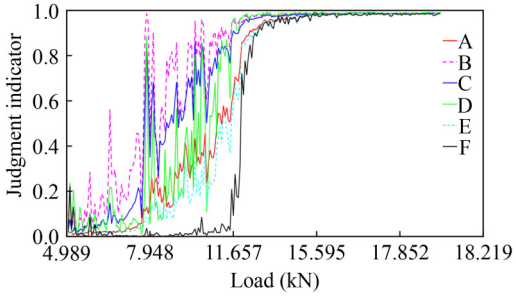

Fig. 14 The judgment curves of the BP neural network

can be seen with the naked eye that for sample No. 214 (the 264th strain nephogram) the convolutional strain nephogram corresponds to a load of 16.877 kN. The judgment indicator of these samples recognized by the convolutional neural network is less than 0.1. Accordingly, after the BP neural network identification of mat file data processed by them, the judgment indicators obtained are all above 0.9, very close to 1.

In addition, the corresponding load of the CNN is 17.603 kN after sample No. 227 (strain nephogram No. 277), and the judgment indicator is stable above 0.7, while the load of the BP neural network is 10.516–11.963 kN between sample No. 85–104 (strain nephogram No. 185–204). The judgment indicator has reached over 0.7, which occurs about 73–92 samples ahead of the same behavior described by the CNN. Strain nephogram No. 277 corresponds to the start of the experiment for 1358 s, No.185 corresponds to 920.5 s, No. 204 corresponds to 1015.5 s. That is, the BP neural network recognition results advance by about 342.5–437.5 s, that is, about 6–7 min. Comparison is summarized in Table 8.

The recognition of CNN is based on images, that is, the strain nephograms themselves, while the recognition by the BP neural network is based on the processed mat file, which contains 7 important parameters of the specimen

Table 8 Comparison of recognition results

Content information	Identify point of convolutional neural network	Identify point of BP neural network
Corresponding strain nephogram number	277	185–204
Load (kN)	17.603	10.156–11.963
Time (seconds)	1358	920.5–1015.5

during the experiment. That is, the recognition method of the CNN described in this paper can provide timely warning of visible cracks. And the BP neural network identification method can predict the possibility of fracture occurrence in an earlier step, when cracks are still invisible.

The trend is developing long before the cracks became visible. For important parts of the component, it is not only necessary to determine the occurrence of cracks by the strain nephogram, but to calculate them and grasp the trend in time.

3.2 Four-point bending test of concrete specimen

3.2.1 Using convolutional neural networks to identify cracks in concrete four-point bending

Details of GoogleNet, as a CNN, are shown in Table 3.

A group of four-point bending experimental data are used, and the images in the data are arranged in chronological order during the experiment. After processing, a total of 50 strain nephograms are obtained. A total of 26 strain nephograms, 1–4 and 29–50, are selected as the training set, of which 1–4 are intact strain nephograms without cracks, corresponding to the load process of 0–0.76 kN, labeled as "negative" and corresponding to the number 0. Nephograms 29–50 are 22 strain nephograms with obvious cracks. The corresponding load process is 7.43–13 kN, labeled as "positive" and corresponding number 1, which is used to train the designed CNN. At the same time, the middle segment of the data, i.e., 5–28 pictures, is selected as the verification set, and the corresponding loading process is 1.06–7.16 kN, as listed in Table 9.

The trained CNN is used to identify the verification set to judge the cracking of four-point bending test specimens. In the training, the network obtains a value between [0,1] on each DIC image of a specimen as the judgment indicator, and the variation of the value of this indicator, between 0 and 1, represents the degree of "negative" and "positive". The smaller the indicator is, the lower the damage degree is and the closer the specimen is to intact. On the contrary, the larger the indicator is, the more obvious the crack development is on the specimen surface.

Table 9 CNN data partitioning

Content information	Training Set (26 in total)		Verification set (24 in total)
Number of strain nephogram	1–4	29–50	5–28
Load process (kN)	0–0.76	7.43–13	1.06–7.16
Judgment indicator	0 (negative)	1 (positive)	to identify [0,1]

The trained CNN recognizes the verification set, and the obtained results are shown in Fig. 15. Since the 5th to 28th images are selected as the verification set, the corresponding sample number of the 5th image is 1, and so on.

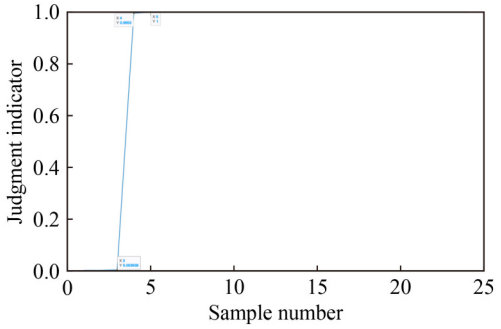

Fig. 15 The judgment curve of CNN.

MSE is 4.337353444 and *RMSE* is 2.082631375.

It can be found that the judgment indicator at the beginning is very stable at a position close to 0. From sample No. 3 to sample No. 4, the judgment indicator leapt from 0.003638 to 0.9953, a sharp increase from close to 0 to close to 1. From sample No. 5, the judgment indicator remained at 1. After the image is rotated, the CNN is used for training and recognition under the same conditions again. After comparison, the image of the judgment indicator obtained remains unchanged.

Meanwhile, sample No. 3 corresponds to the 7th strain nephogram, with a load of 1.59 kN, as shown in Fig. 16.

There are few cracks at this point, and a closer look reveals a subtle crack beginning in the lower-left corner of the image.

Sample No. 4 corresponds to the 8th strain nephogram, with a load of 1.86 kN, as shown in Fig. 17.

It can be observed from the strain nephogram that the fracture in the lower-left corner of sample 8 developed further and became more obvious, while the fracture in the lower right corner also started. The judgment indicator of the BP neural network is very sensitive to this point.

Sample No. 5 corresponds to the ninth strain nephogram, with a load of 2.12 kN, as shown in Fig. 18.

At this point, the judgment indicator of the CNN is very certain and remained stable at 1. Meanwhile, the crack in the lower-left corner expanded and showed more integrity, while the crack in the lower right corner became thicker and the cracking characteristics are very obvious. The judgment indicator is consistent with the actual situation.

To facilitate observation, the situation after further development of cracks is presented. In all 50 strain nephograms, the 50th strain nephogram, with a load of 13 kN, as shown in Fig. 19.

It can be found that the well-trained CNN is very sensitive to crack warning according to the judgment indicator graph obtained from the neural network mentioned above and the actual strain nephogram. Although the cracks in the figure are small, the jump of the judgment indicator is very sensitive and the cracks are found in real-time, which is consistent with the actual situation. After the image is rotated, the CNN is used for training and recognition under the same conditions again, and the obtained image of the judgment indicator remains unchanged.

Therefore, in the actual possible application, we should pay close attention to the image of the judgment indicator, and pay attention to the situation of the relevant parts when there is a fluctuation and a rising trend, to avoid the further expansion of cracks and affect the strength of the structure. In addition, when the CNN is used for recognition, the angle of the picture has little influence on its judgment indicator, that is, it does not have strict requirements on the lens placement angle of the camera, which is convenient for practical application.

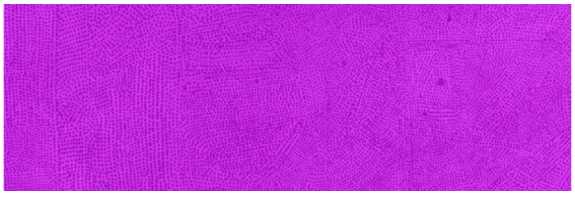

Fig. 16 The first principal strain nephogram of the load at 1.59 kN.

Fig. 17 The first principal strain nephogram of the load at 1.86 kN.

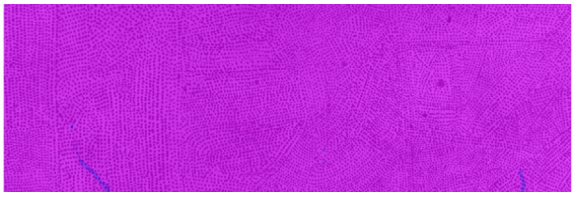

Fig. 18 The first principal strain nephogram of the load at 2.12 kN.

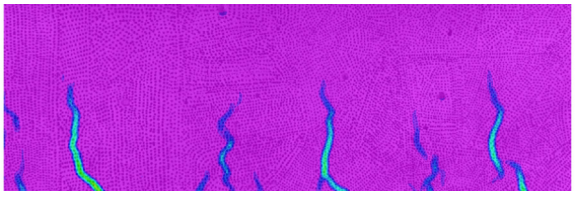

Fig. 19 The first principal strain nephogram of the load at 13 kN.

3.2.2 Using back propagation neural network to identify cracks in concrete three-point bending

The BP neural network is constructed to identify concrete damage. At the beginning of training, the weighting is random. The momentum factor is 0.03, the learning rate is 0.01, the error tolerance is 0.01, and the maximum iteration number is 2000. The hyper-parameters of the BP are listed in Table 10. When the sum of error squares is less than error tolerance, iteration is stopped; otherwise, iteration continues until the maximum number of iterations is reached, and then iteration is stopped.

Table 10 The hyper-parameters of the BP

Hyper-parameter	Value
Momentum factor	0.03
Learning rate	0.01
Error tolerance	0.01
Maximum iteration	20000

The BP neural network is trained with different parameters, including only the first principal strain ε_1, only the second principal strain ε_2, only the x-direction strain ε_{xx}, only the y-direction strain ε_{yy}, only the shear strain ε_{xy}, and all the above strains. It is also trained with only the horizontal displacement u, only the longitudinal displacement v, all the aforementioned displacements u and v. Finally, all parameters , ε_1, ε_2, ε_{xx}, ε_{yy}, ε_{xy}, u, v are used. The selected parameters are listed in Table 11.

Mat files 1–10 and 51–60 are selected as a total of 20 as training sets. Among them, 1–10 is not cracked and labeled as “0”, while 51–60 are cracked, labeled as “1”. At the same time, the 11th to 50th mat files are selected as a total of 40 as verification sets, as listed in Table 12.

The BP neural network is trained with the data of the training set, and the trained BP neural network recognizes the data of the verification set, and the recognition results are drawn to obtain the image of the judgment indicator.

The training situation is shown in Fig. 20, where the horizontal axis is the sample label corresponding to the load size, and the vertical axis is the failure degree judgment indicator, and the failure degree increases with the increase from 0 to 1. Parameters of different combinations are selected as the input of the network, and the

Table 11 Parameter selection

Number of the selected group	The first principal strain ε_1	The second principal strain ε_2	Strain in x-direction ε_{xx}	Strain in y-direction ε_{yy}	Shear strain ε_{xy}	Horizontal displacement u	Longitudinal displacement v
A	√						
B		√					
C			√				
D				√			
E					√		
F	√	√	√	√	√		
G						√	
H							√
I						√	√
J	√	√	√	√	√	√	√

Table 12 BP neural network data partitioning

Content information	Training Set (20 in total)	Verification set (24 in total)
Number of mat files	1–10, 51–60	11–50
Load process (kN)	0–2.39, 13	2.65–13
Judgment indicator	0 (negative), 1 (positive)	to identify [0,1]

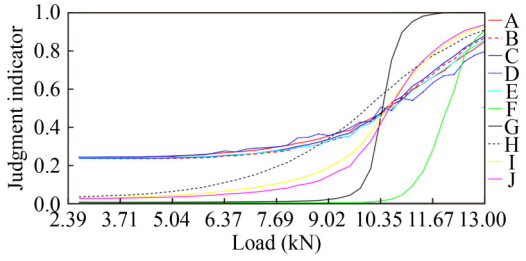

Fig. 20 The judgment curves of the BP neural network.

judgment result is obtained after the operation. The closer the judgment value is to 0, the more the corresponding sample tends to the set labeled "0", that is, the lower is the level of cracking. Conversely, the closer it is to 1, the more the corresponding sample tends to the set labeled "1"; that is, the crack tends to appear.

The K-fold cross validation technique is adopted to help to evaluate the model to avoid a high variance and bias in the results generated. The MSE is 0.5% and the RMSE is 0.707107%.

After analyzing the images above, we can see that comparing the two judgment images obtained by selecting the strain parameters in the x-direction and the strain parameters in the y-direction, and that compared with selecting the strain parameters in the y-direction, the judgment indicator in the graph obtained by selecting the strain parameters in the x-direction is slightly smaller at the beginning. According to the material mechanics formula,

$$\varepsilon_{xx} = -\mu\varepsilon_{yy}. \quad (1)$$

Poisson's ratio $\mu < 1$, so the judgment indicator graph obtained by selecting strain parameters in the y-direction is slightly larger than that obtained by selecting strain parameters in the x-direction.

In addition, in the judgment indicator curve, the slope obtained by selecting horizontal displacement is larger than that of longitudinal displacement, and selecting strain in the x-direction is larger than that in the y-direction. Considering the curve itself, the larger and steeper slope means that the damage degree reflected by the selected parameters is more obvious, and the slight change has a greater impact on the judgment indicator. At the same time, considering the characteristics of the concrete itself, its tensile strength is greater than the compressive strength. Compared with the longitudinal direction, when the displacement and strain increase in the horizontal direction, the damage of concrete specimens is greater, and then cracks appear.

It can be found that the judgment indicator charts obtained by selecting the horizontal displacement parameters are all 0 at the beginning, or close to 0, while the first end of the judgment indicator charts obtained by longitudinal displacement is not 0. This situation may be the testing machine bearing in the longitudinal rigid body displacement.

Comparing the three-point bending and four-point bending experiments of concrete, when selecting different parameters to get judging indicator images, it can be found that the four-point bending of the image is smoother, with fewer fluctuations than in the case of three-point bending experiment data. Besides the error caused by the unstable machine itself, this kind of situation may also be related to the concrete specimen itself. In the three-point bending experiment, plain concrete specimens are poured, while in the four-point bending experiment, reinforced concrete specimens are used. Due to the reinforcement effect of steel bars, the stress on the specimens in the loading process is more uniform, which reduces the noise in the data to a certain extent, and the final judgment indicator image is smoother.

Compared with the recognition curves obtained by training with different parameter groups, the recognition curve obtained by training with single strain parameter is relatively flat, and it is difficult to judge whether a specimen is cracked, while the recognition curve obtained by training with displacement parameter is relatively steep. Due to the comprehensive consideration of the ductility of the steel bar and the brittleness of the concrete, there is a process of cracking of reinforced concrete in the four-point bending experiment. Therefore, the slope of the curve obtained by training with the combination of the displacement and strain parameters is moderate. A more comprehensive consideration makes its judgment more objective and comprehensive, avoiding rough judgment.

4 Conclusions

This paper mainly aims at the crack identification of the concrete specimens. Since DIC technology can provide a large amount of experimental data, and NN can handle very rich data, NN is combined with DIC technology to summarize the rules in the large amount of data, so as to make the results more objective. The identification results are made more comprehensive by combining strain and displacement parameters. The parameters obtained by DIC technology are grouped for training, and the recognition results of NN are observed to find the grouping more suitable for crack identification in engineering. In addition, the comparison of recognition results of the CNN and the BP shows that these two tools are applicable to different conditions, so they can embody their advantage in different situations, and can play an important role in engineering monitoring. The main research contents and results are as follows.

1) DIC technology can provide a large amount of experimental data, while NN can process very rich data. The results show that the NN can be combined with DIC technology to analyze the rules in the data, and get more objective and comprehensive conclusions.

2) A large amount of data obtained by DIC technology is used for NN training. The recognition results of the CNN and the BP are accurate and realistic. It can be seen that strain reflects the response of the surface of the specimens, and displacement reflects the response of the specimen as a whole. Combining these two factors can make the judgment more comprehensive and objective.

3) It can be found that the CNN can directly identify images, which is relatively convenient, but the cracks identified are mostly formed through macro development, which is suitable for occasions with low accuracy. The BP can identify cracks earlier and give early warning to microscopic cracks, but it requires a large amount of data and large amount of calculation, and can be applied to the occasion of high precision. They can be applied to different damage scenarios more comprehensively, to use their advantages for different scenarios and play an important role in engineering monitoring.

Although the NN can analyze data effectively and help make objective and comprehensive judgment, it also has some limitations. GoogLeNet, for example, is limited by depth and complexity. The complexity of the network increases the difficulty of training, and a large number of parameters in the network may lead to overfitting, which will limit the generalization ability of the network. Due to the fixed learning rate of BP neural network, the convergence rate of BP neural network is slow and it takes a long time to train. When used for function approximation, the negative gradient descent method is used to adjust the weight, which may lead to slow convergence and local minimum.

Acknowledgements The financial supports for this research are provided by the National Natural Science Foundation of China (Grant Nos. U1765204 and 51679078) and the Research and Innovation Plan for Postgraduates in Jiangsu Province (No. KYCX21_0458). Their contributions are gratefully acknowledged.

Competing interests The authors declare that they have no competing interests.

References

1. Zhang J, Song Z, Bing H, Xie H, Li P. Research progress on fatigue of highway concrete bridges under vehicle loading. China Civil Engineering Journal, 2023, 55(12): 65−79 (in Chinese)
2. Liu X, Sun Q H, Song W, Bao Y H. Structural behavior of reinforced concrete tunnel linings with synthetic fibers addition. Tunnelling and Underground Space Technology, 2023, 131: 104771
3. Mishra M, Lourenco P B, Ramana G V. Structural health monitoring of civil engineering structures by using the internet of things: A review. Journal of Building Engineering, 2022, 48: 103954
4. Koike K, Yamaji T, Nishida T, Yonamine K, Adachi A, Nakagawa K. Influence of transportation and pumping on the properties of concrete with large amount of copper slag fine aggregate in actual construction of port and harbor structures. Journal of Material Cycles and Waste Management, 2022, 24(4): 1368−1377
5. An Q, Chen X J, Wang H J, Yang H M, Yang Y J, Huang W, Wang L. Segmentation of concrete cracks by using fractal dimension and UHK-Net. Fractal and Fractional, 2022, 6(2): 95
6. Chauhan A, Sharma U K. Identifying factors influencing corrosion rate in reinforced concrete under simulated natural climate. Current Science, 2022, 123(11): 1327−1333
7. Zhao B N, Dong L, Fu J J, Yang L Q, Xu W X. Experimental study on micro-damage identification in reinforced concrete beam with wavelet packet and DIC method. Construction & Building Materials, 2019, 210: 338−346

8. Huang Y Y, Zheng H, Zhou Y H. Study of concrete block's thermal stress considering tensile and pressure different creep. Journal of Wuhan University of Technology, 2011, 33(3): 87−92 (in Chinese)
9. Liang S Y. Review on concrete cracking and maintenance. Sichuan Cement, 2016, 38(7): 262
10. Tong Z N, Gao Y. Cause and influence of mass concrete crack. International Conference on Chemical, Material and Food Engineering. 2015, 22:497–499
11. Zhou S L, Zhao Q, Guo J Q. Analysis and control technology of hydraulic concrete crack. Water Resources Planning and Design, 2021(4): 110−114
12. Luo G H, Pan J W, Wang J T. Study on the influence factors of Rayleigh wave method for detecting the crack depth of concrete Surface. Water Resources and Hydropower Technology, 2021, 52(9): 165−171
13. Liu X Z. Laser ultrasonic detection method for crack depth of concrete. Journal of Central South University (Science and Technology), 2021, 52(3): 839−847 (in Chinese)
14. Wei S H, Liu Y F, Liu J H. Research on surface crack detection of concrete structure based on UAV and digital image method. Special Structures, 2020, 37(5):107–111
15. Li Y W, Xiang H, Peng W. Research and application of high dam concrete crack detection technology based on UAV and underwater robot. Building Technology Development, 2021, 48(3): 52−54
16. Cheng L, Tian G Y. Surface crack detection for carbon fiber reinforced plastic (CFRP) materials using pulsed eddy the current thermography. IEEE Sensors Journal, 2011, 11(12): 3261−3268
17. Zhang L X, Shen J K, Zhu B J. A review of the research and application of deep learning-based computer vision in structural damage detection. Earthquake Engineering and Engineering Vibration, 2022, 21(1): 1−21
18. Huang H W, Li Q T, Zhang D M. Deep learning based image recognition for crack and leakage defects of metro shield tunnel. Tunnelling and Underground Space Technology, 2018, 77: 166−176
19. Ma X L, Lu J. Research on Road Surface Crack Image Classification Algorithm Based on Grayscale Analysis. Journal of Wuhan University of Technology (Traffic Science and Engineering), 2018, 42(5): 748−752, 756 (in Chinese)
20. Chai X S, Zhu X Y, Li J C, Xue F, Xin X S. Tunnel lining crack recognition algorithm based on deep convolutional neural network. Railway Construction, 2018, 58(6): 60–65
21. Zhang Z D, Jung C. GBDT-MO: Gradient-boosted decision trees for multiple outputs. IEEE Transactions on Neural Networks and Learning Systems, 2021, 32(7): 3156−3167
22. Vieira F, Taveira-Pinto F, Rosa-Santos P. Novel time-efficient approach to calibrate VARANS-VOF models for simulation of wave interaction with porous structures using artificial neural networks. Ocean Engineering, 2021, 235: 103975
23. Alazzam M B, Hajjej F, AlGhamdi A S, Ayouni S, Rahman M A. Mechanics of materials natural fibers technology on thermal properties of polymer. Advances in Materials Science and Engineering, 2022, 2022: 1−5
24. Ghasemi A, Amirabadi R, Kamalian U R, Mazyak A R. Numerical modeling investigation of perforated geometry of caisson breakwater under irregular waves by considering porous media. Ocean Engineering, 2023, 269: 113558
25. Li M Z, Yan R J, Xu L, Soares C G. A general framework of higher-order shear deformation theories with a novel unified plate model for composite laminated and FGM plates. Composite Structures, 2021, 261: 113560
26. Le-Duc T, Nguyen Q H, Nguyen-Xuan H. Balancing composite motion optimization. Information Sciences, 2020, 520: 250−270
27. Farzam A, Hassani B. Isogeometric analysis of in-plane functionally graded porous microplates using modified couple stress theory. Aerospace Science and Technology, 2019, 91: 508−524
28. Dang B L, Nguyen-Xuan H, Wahab M A. An effective approach for VARANS-VOF modelling interactions of wave and perforated breakwater using gradient boosting decision tree algorithm. Ocean Engineering, 2023, 268: 113398
29. Girshick R. Fast R-CNN. In: Proceedings of the International Conference on Computer Vision. Xi'an: IEEE, 2015, 1440–1448
30. Tran V T, Nguyen T K, Nguyen-Xuan H, Wahab M A. Vibration and buckling optimization of functionally graded porous microplates using BCMO-ANN algorithm. Thin-walled Structures, 2023, 182: 110267
31. Kilic H, Yuzgec U, Karakuzu C. Improved antlion optimizer algorithm and its performance on neuro fuzzy inference system. Neural Network World, 2019, 29(4): 235−254
32. Yuan S C. Review of root-mean-square error calculation methods for large deployable mesh reflectors. International Journal of Aerospace Engineering, 2022, 2022: 5352146
33. Ho L V, Trinh T T, de Roeck G, Bui-Tien T, Nguyen-Ngoc L, Abdel Wahab M. An efficient stochastic-based coupled model for damage identification in plate structures. Engineering Failure Analysis, 2022, 131: 105866
34. Guo H W, Zhuang X Y, Chen P W, Alajlan N, Rabczuk T. Stochastic deep collocation method based on neural architecture search and transfer learning for heterogeneous porous media. Engineering with Computers, 2022, 38(6): 5173−5198
35. Guo H W, Zhuang X Y, Chen P W, Alajlan N, Rabczuk T. Analysis of three-dimensional potential problems in non-homogeneous media with physics-informed deep collocation method using material transfer learning and sensitivity analysis. Engineering with Computers, 2022, 38(6): 5423−5444
36. Hu HP, Yang Y. A combined GLQP and DBN-DRF for face recognition in unconstrained environments. In: Proceedings of the 2nd International Conference on Control, Automation and Artificial Intelligence. Paris: Atlantis Press, 2017, 553–557
37. Nayoung K, Min K Y, Ko S. Performance improvement method of convolutional neural network using agile activation function. KIPS Transactions on Software and Data Engineering, 2021, 9(7): 213−220
38. Svozil D, Kvasnicka V, Pospichal J. Introduction to multi-layer feed-forward neural networks. Chemometrics and Intelligent Laboratory Systems, 1997, 39(1): 43−62
39. Guo M G, Gong H. Research on AlexNet improvement and optimization method. Computer Engineering and Application., 2021, 56(20): 124−131

40. Chan K H, Im S K, Ke W. VGGreNet: A Light-Weight VGGNet with Reused Convolutional Set. In: Proceedings of the 13th International Conference on Utility and Cloud Computing (UCC). IEEE, 2020: 434–439
41. Peng D L, Wang T X. Pruning algorithm based on GoogLeNet model. Control and Decision, 2019, 34(6): 1259−1264
42. Su Y, Song J X. A detection method based on Bayesian hierarchical network for abnormal interaction. In: Proceedings of the 2016 4th International Conference on Advanced Materials and Information Technology Processing (AMITP 2016). Lima: Atlantis Press, 2016, 60: 333−340
43. Tan M, Quoc L. Efficientnet: Rethinking model scaling for convolutional neural networks. In: Proceedings of the International Conference on Machine Learning. Long Beach, CA: PMLR, 2019, 6105–6114
44. Xu J C, Zhang J K, Shen Z Z. Recognition method of internal concrete structure defects based on 1D-CNN. Journal of Intelligent & Fuzzy Systems, 2022, 42(6): 5215−5226
45. Wang B X, Zhao W G, Gao P, Zhang Y F, Wang Z. Crack damage detection method via multiple visual features and efficient multi-task learning model. Sensors, 2018, 18(6): 1796
46. Zhang X Q, Akber M Z, Zheng W. Predicting the slump of industrially produced concrete using machine learning: A multiclass classification approach. Journal of Building Engineering, 2022, 58: 104997